Journal of Applied Polymer Science

Thermal and Flammability Performance of Polypropylene Composites Containing Melamine and Melamine Phosphate-Modified α-Type Zirconium Phosphates

Deng Liu,[1] Guipeng Cai,[2] Juan Wang,[1] Xiaofang Tan,[1] Hongdian Lu,[1] Shiyun Zhang,[1] Qingqing Dai[1]
[1]Department of Chemical and Materials Engineering, Hefei University, Hefei, Anhui 230601, People's Republic of China
[2]Department of Chemistry and Fire Retardant Research Facility, Marquette University, Milwaukee, Wisconsin 53201
Correspondence to: H. Lu (E-mail: hdlu@ustc.edu.cn)

ABSTRACT: In this article, melamine (MA) and melamine phosphate (MP) have been intercalated into α-type zirconium phosphate (α-ZrP) interlayer spaces. The structure and thermal properties of the corresponding powders, MA-ZrP and MP-ZrP, were ascertained by X-ray diffraction, Fourier transform infrared spectra, X-ray photoelectron spectroscopy measurement, and thermogravimetric analyses (TGA). Furthermore, polypropylene (PP) and its intumescent flame retardant (IFR) composites containing the two organically modified α-ZrP powders using maleic anhydride-grafted PP (JPP) as compatibilizer were fabricated by melt blending. The results from TGA and cone calorimetry demonstrated that PP/JPP and PP/JPP/IFR composites containing MA-ZrP and MP-ZrP exhibited better thermal stability and burning behavior in comparison with their corresponding counterparts, PP/JPP and PP/JPP/IFR, respectively. © 2013 Wiley Periodicals, Inc. J. Appl. Polym. Sci. **2014**, *131*, 40254.

KEYWORDS: thermal properties; degradation; flame retardance; nanostructured polymers; structure-property relations

Received 26 October 2013; accepted 3 December 2013
DOI: 10.1002/app.40254

INTRODUCTION

Layered compounds such as montmorillonite (MMT) clay and zirconium phosphates (ZrPs) are potential flame retardant additives for polymers.[1–4] By forming intercalated and/or delaminated nanostructure, these nanoparticles, at minimal addition levels, impart polymer/layered compounds nanocomposites with improved thermal stability, barrier properties, and fire retardancy. Typically, a substantial decrease in peak heat release rate (HRR) can be achieved for a variety of polymer nanocomposites when tested by cone calorimetry.

α-Type ZrP (α-ZrP) possesses high Bronsted acidity and a controllable aspect ratio; it has shown promise to enhance flammability performance of polymer nanocomposites such as polystyrene (PS) and polyvinyl alcohol.[5,6] Unlike the commonly used clay, MMT, α-ZrP is postulated to contribute to the improved flammability performance mainly through catalytic carbonization effect, rather than physical effects, by forming a high-performance carbonaceous char on the sample surface.

Although polymer nanocomposites exhibit improved flammability performance and decreased HRR peak in cone calorimetry, they cannot obtain a classification in some standard fire tests, such as limited oxygen index or the UL-94 vertical burning tests. Combination of traditional flame retardants, including halogen and halogen-free, with nanocomposites has been to an efficient way to solve the problem, due to the synergy that can occur between layered compounds and flame retardants.[7–10] Among the flame retardants, the intumescent flame retardant (IFR) system is a widely used halogen-free flame retardant additive. The IFR system is commonly composed of three components, an acid source, such as ammonium polyphosphate and melamine polyphosphate (MPP), a charring agent commonly polyols, such as pentaerythritol (PER), and a blowing agent, such as melamine (MA). The intumescent char generated during the combustion process is believed to act as a physical barrier to slow heat and mass transfer between the gas and condensed phases. As for synergy, the combination of IFR with organically modified MMT and α-ZrP in polypropylene (PP), PS, and so on, leads to polymeric materials that yield more stable residual char and imparts better flame retardancy.[11–14]

Commonly, the intercalation agents used to modify layered compounds are long-chain quaternary alkylammonium salts, but using one of the components of the IFRs as an intercalation agent to modify layered compounds and investigate their effect on thermal degradation and combustion behavior of polymers is the goal of this work. In this article, two kinds of organically modified ZrPs (OZrPs), MA and melamine phosphate (MP) modified α-ZrP, forming MA-ZrP and MP-ZrP, respectively, that were

prepared via a batch method. PP composites with the two powders were prepared and the effect of the combination of IFR with these powders on flame retardancy was studied. The aim was to investigate the influence of MA-ZrP and MP-ZrP on thermal stability and flammability performance of PP composites.

MATERIALS AND METHODS

Materials

PP homopolymer resin (HP 500N, melt flow rate 12 g/10 min (230°C/2.16 kg) was supplied by CNOOC and Shell Petrochemicals Co. Ltd. The maleic anhydride-grafted PP (JPP) with approximately 1.0 wt % maleic anhydride was kindly provided by Keyan Chemistry Co. Zirconyl chloride ($ZrOCl_2{\cdot}8H_2O$), phosphoric acid (H_3PO_4, ≥85%, solution in water), MA ($C_3N_6H_6$), and PER were supplied by Sinopharm Chemical Reagent Co. Ltd. MP ($C_3N_6H_9O_4P$) and MPP were provided by Hefei Finecollection Institute of Chemical Industry. All chemicals were used as received without further purification.

Preparation

α-ZrP was synthesized by refluxing $ZrOCl_2{\cdot}8H_2O$ in 10 mol/L H_3PO_4 for 24 h at 95°C as described by Sun et al.[15] The intercalation of MA and MP into α-ZrP was carried out by a batch method in which an aqueous MA or MP solution (1 g/100 g) was added to an α-ZrP water suspension (1 g/100 g) then stirred at 80°C for 24 h. The precipitate was centrifuged and washed using 80°C deionized water. The samples were dried at 60°C then ground and sieved to 300 mesh.

PP composites with JPP as compatibilizer (85/15 by weight) containing 6 phr (part of reagent per hundred parts of polymeric matrix) additive, MA-ZrP and MP-ZrP, were melt compounded using a Brabender mixer at 180°C for 10 min at a screw speed of 90 rpm. To obtain PP/JPP/IFR/MA-ZrP and PP/JPP/IFR/MP-ZrP composites, MA-ZrP and MP-ZrP were first melt blended with the polymeric matrix for 5 min, then IFR (MPP/PER = 3/1 by weight) was added and mixed for an additional 8 min. The formulations are shown in Table I.

Table I. Formulations and TGA Data Tested in a Nitrogen Atmosphere of PP and Its IFR Flame Retarded Composites

Sample	$T_{5\%}$ (°C)	T_{max} (°C)	Char (%, 550°C)
PP/JPP	419	462	1.5
PP/JPP/MA-ZrP[a]	429	460/468[b]	5.5
PP/JPP/MP-ZrP[a]	433	460/470	4.9
PP/JPP/ IFR(25)[c]	297	246/422/500	6.8
PP/JPP/MA-ZrP(2)/ IFR(23)	303	243/468/515	7.8
PP/JPP/MP-ZrP(2)/ IFR(23)	315	243/465/515	8.0

$T_{5\%}$, temperature at which 5% degradation occurs; T_{max}, temperature obtained from DTG curves at which the maximum mass loss rate occurs; Char, the fraction of the residue remaining at 550°C.
[a] 6 phr MA-ZrP or MP-ZrP was contained in PP/JPP polymeric matrix.
[b] Temperature at which the maximum mass loss rate occurs during different thermal degradation stages.
[c] 25 phr IFR (MPP/PER = 3/1) was contained in PP/JPP polymeric matrix.

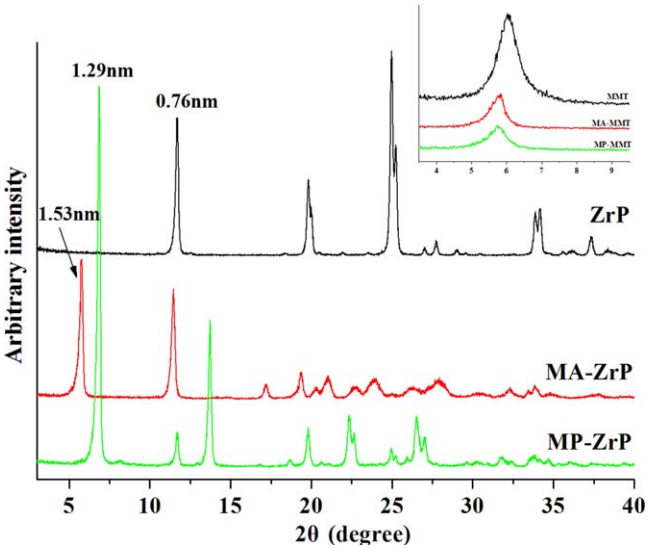

Figure 1. XRD patterns of ZrP, MA-ZrP, and MP-ZrP powders. The insert shows that the intercalation of MA and MP into MMT leads to a very little increase in interlayer distance. [Color figure can be viewed in the online issue, which is available at wileyonlinelibrary.com.]

Characterization

The X-ray diffraction (XRD) data were obtained at room temperature using a Rigaku D-Max-Ra rotating anode X-ray diffractometer equipped with a Cu-K_α tube and a Ni filter ($\lambda = 1.5402$ Å). TEM images were obtained using a JEOL JEM-2100 transmission electron microscope with an acceleration voltage of 200 kV. The PP composite specimens were microtomed to ultrathin sections using a Du Pont MT-6000 Ultratome and transferred onto copper grid for observation. The Fourier transform infrared spectra (FTIR) were obtained using a Nicolet MAGNA-IR 750 spectrometer with a resolution of 4 cm^{-1} for the characterization of MA-ZrP and MP-ZrP powders. The X-ray photoelectron spectroscopy measurement (XPS) was carried out using an ESCALABMK II spectrometer, with Al k_α excitation radiation ($h\nu = 1253.6$ eV) in ultra-high vacuum conditions. Thermogravimetric analyses (TGA) were conducted with a TA Q5000 thermoanalyzer instrument. In each case, 5 mg specimens were heated from 30 to 600°C at a heating rate of 10°C/min in a nitrogen atmosphere at a flow rate of 40 mL min^{-1}. The cone calorimeter experiments were carried out using an Atlas Cone 2 instrument according to ASTM E 1354, on 3-mm-thick 100 × 100 mm^2 plaques. The cone data obtained are reproducible to within ±10% when measured at a heat flux of 35 kW/m^2.

RESULTS AND DISCUSSION

Characterization of MA-ZrP and MP-ZrP Powders

Figure 1 displays the XRD patterns of α-ZrP, MA-ZrP, and MP-ZrP powders. α-ZrP shows the 002 diffraction peak at $2\theta = 11.7°$ with a basal interlayer spacing of 0.76 nm. The intercalation of MA and MP into α-ZrP leads to an increase in interlayer distance to 1.53 nm and 1.29 nm, respectively, coexisting with the original 002 reflection peak of α-ZrP, which indicates that MA and MP are partially intercalated inside the phosphate gallery space. Similar to the report,[16] the increment in interlayer distance, 0.77 nm (1.53–0.76) in MA-ZrP sample, suggests that MA forms a bilayer structure with two protonated amino

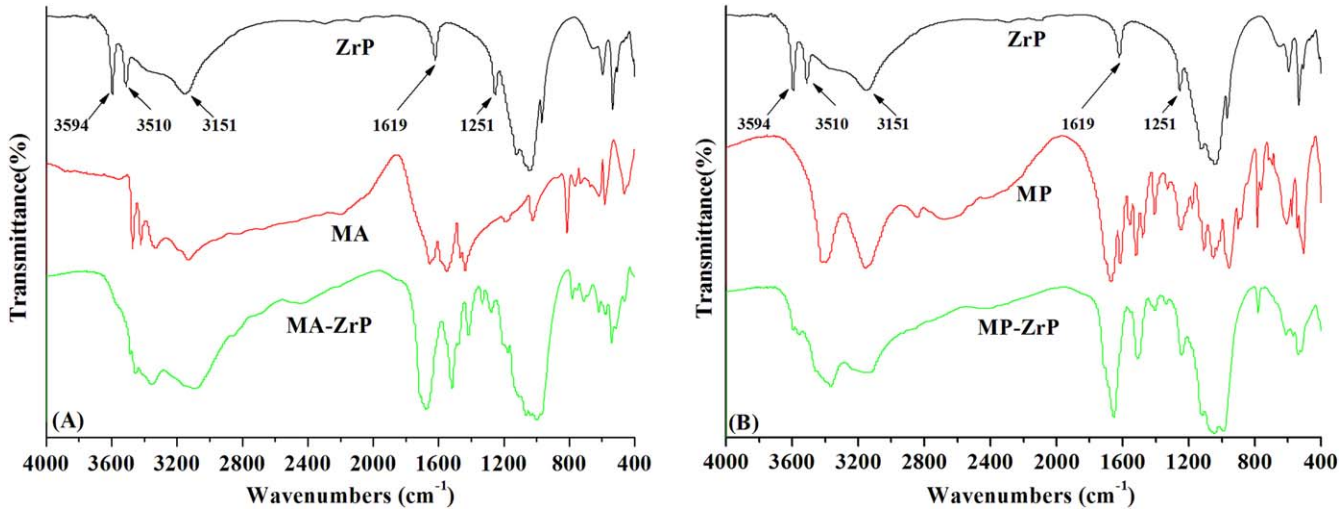

Figure 2. FTIR spectra of MA-ZrP and MP-ZrP powders. [Color figure can be viewed in the online issue, which is available at wileyonlinelibrary.com.]

groups adjacent to phosphate layers; while for MP-ZrP, the 0.53 nm increment may suggest that a monolayer structure is formed.

The FTIR spectra of α-ZrP, MA-ZrP, and MP-ZrP powders are shown in Figure 2. α-ZrP shows the characteristic PO_4^{3-} absorption bands in the range of 968–1124 cm^{-1}.[17] The absorption bands at 3594 and 3510 cm^{-1} are assigned to the antisymmetric stretching vibration of interlayer crystalline water, which are shifted to lower frequency and broaden in MA-ZrP and MP-ZrP, suggesting that water is expelled from the interlayer spaces. The bands at 3151 and 1251 cm^{-1} are ascribed to P—OH stretching and deformation vibrations of phosphate hydroxyl. The two peaks disappear in both MA-ZrP and MP-ZrP samples after interaction, which suggests that the bond are generated between amino groups of MA or MP and P—OH group of phosphate layers to form a —C—NH_3^+—O—P— assembly; also hydrogen bridges between hydroxyl of MP and P—OH group of phosphate layers may occur, as shown in Scheme 1.

The decomposition of MA-ZrP and MP-ZrP has an important role in the thermal degradation of their corresponding polymeric composites; the TG-derivative TG (DTG) curves of MA and MP intercalated α-ZrP compounds are shown in Figure 3. α-ZrP undergoes a dehydration process with the maximum weight loss temperature at around 140°C, followed by a condensation reaction of the monohydrogen phosphate (P—OH) to pyrophosphate at 570°C.[18] MP-ZrP exhibits a lower mass loss rate and higher thermal stability in the tested temperature range in comparison with MA-ZrP. It can be seen that both of the samples start to lose the physically absorbed water around 150°C; with increasing temperature to 600°C, 18% weight loss

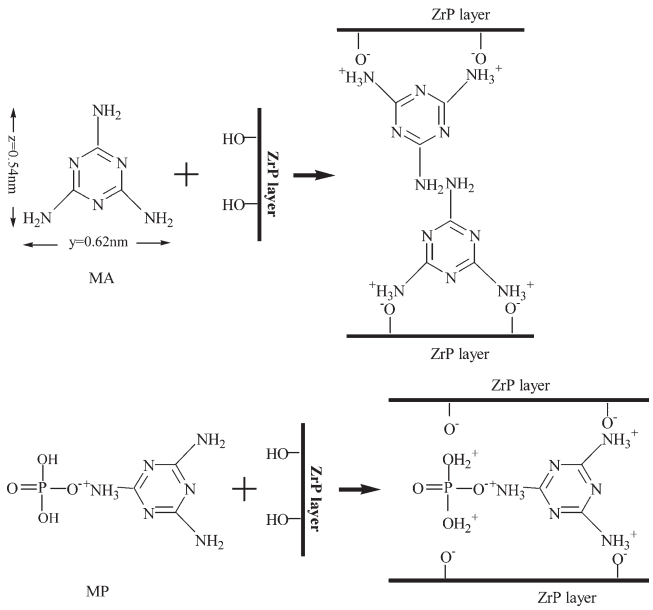

Scheme 1. Illustration of the formation of new bonds between MA or MP and phosphate layers. MP was supposed to face the phosphate layer to inclined to form an angle 58.7°, which was calculated by 0.62 $\sin\theta = 0.53$.

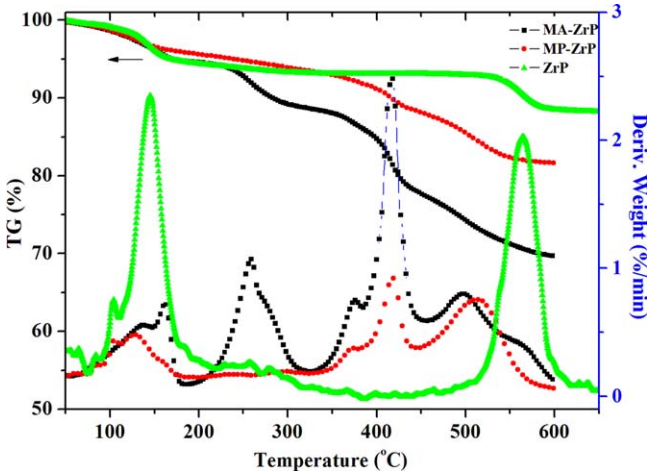

Figure 3. TGA and DTG curves of MA-ZrP and MP-ZrP powders. [Color figure can be viewed in the online issue, which is available at wileyonlinelibrary.com.]

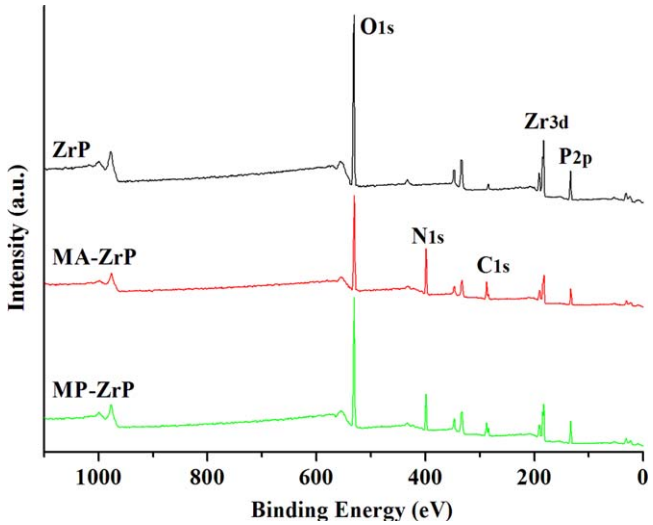

Figure 4. XPS spectra of ZrP, MA-ZrP, and MP-ZrP powders. [Color figure can be viewed in the online issue, which is available at wileyonlinelibrary.com.]

occurs in MP-ZrP, due to the degradation of MP, leading to the formation of ultraphosphate structure with the release of NH_3 gases and water vapor; 30% weight loss occurs in MA-ZrP, caused by the higher uptake amount of MA in α-ZrP.

XPS spectra were used to determine the surface elemental compositions of MA and MP intercalated α-ZrP (Figure 4); the corresponding data are listed in Table II. α-ZrP shows peaks at 531.7 eV, 183.4 eV, and 133.9 eV, which are ascribed to O_{1s}, Zr_{3d}, and P_{2p}, respectively. In the intercalated samples, a new peak centered at about 399.0 eV attributed to N_{1s} appears. As listed in Table I, the carbon and nitrogen contents are increased, but oxygen, zirconium, and phosphate atom contents are decreased in both MA-ZrP and MP-ZrP when compared with α-ZrP. The results indicate that the surfaces of α-ZrP nanoplatelets are partially covered by MA or MP. Furthermore, it can be seen that MA-ZrP has lower Zr atom percentage than MP-ZrP, which may due to the formation of bilayer structure in MA-ZrP leading to more MA molecularly bonded onto the phosphate layers.

Table II. The Surface Elemental Compositions of OZrP Powders

	Elemental content (%)				
Sample	C_{1s}	O_{1s}	N_{1s}	P_{2p}	Zr_{3d}
ZrP	5.99	72.56	0.64	14.26	6.55
MA-ZrP	18.19	41.96	28.07	7.94	3.84
MP-ZrP	15.79	49.56	19.82	10.08	4.76

Morphological Structure of PP Composites

TEM was used to observe the dispersion of modified α-ZrP particles in the PP/JPP matrix (Figure 5). As shown in Figure 5($A1_1$,$B1_1$), MA-ZrP and MP-ZrP particles are dispersed homogeneously throughout the matrix. While in Figure 5($A2_2$,$B2_2$) at higher magnification, the presence of both individual and stacked MA-ZrP and MP-ZrP nanoplatelets in the matrix can be found, which suggests a mixed intercalated-exfoliated nanostructure. Meanwhile, some immiscible components are also observed in this nanostructure.

Thermal Stability of PP Composites

The influence of MA-ZrP and MP-ZrP on the thermal decomposition of PP composites was evaluated by TGA (Figure 6). The mass loss at 5% degradation, $T_{5\%}$, taken as the onset temperature of degradation, T_{max}, the temperature of the maximum mass loss rate obtained from DTG curves, and the fraction of

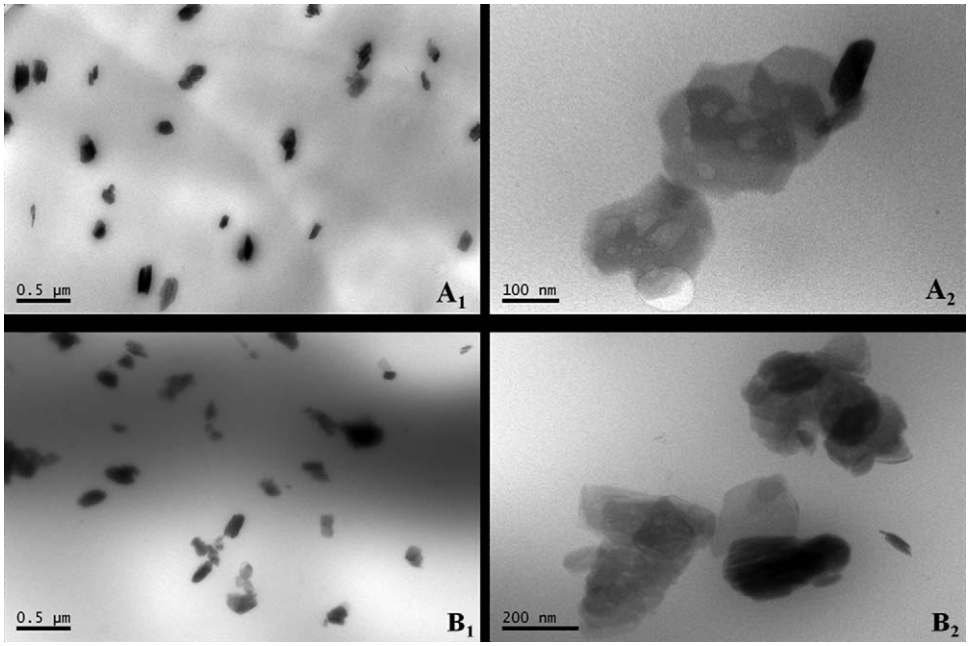

Figure 5. TEM images of composites (A) PP/JPP/MA-ZrP and (B) PP/JPP/MP-ZrP at different magnifications.

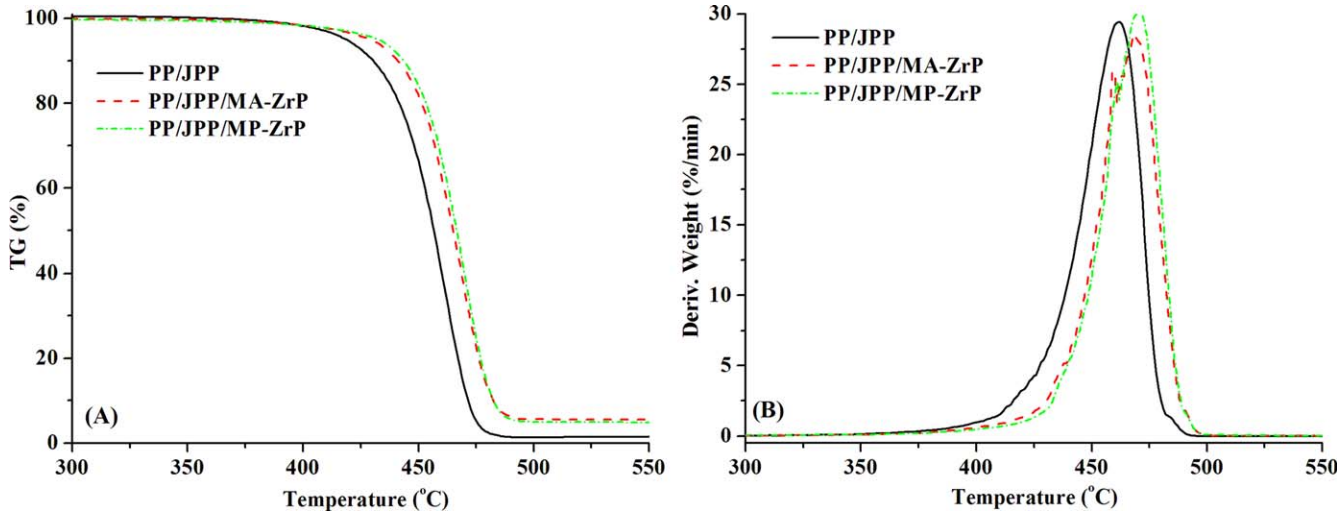

Figure 6. TGA and DTG curves of PP/JPP, PP/JPP/MA-ZrP, and PP/JPP/MP-ZrP composites. [Color figure can be viewed in the online issue, which is available at wileyonlinelibrary.com.]

the residue remaining at 550°C, referred to as char, are listed in Table I.

The decomposition of PP/JPP blend occurs in a single step, starting at 419°C with the maximum mass loss rate at 462°C, and leaves 1.5% residual char at 550°C. For PP/JPP/MA-ZrP and PP/JPP/MP-ZrP samples, the hybrids begin to lose mass at higher temperature (430°C) and are about 10°C more thermally stable compared with PP/JPP blend in the range 420–490°C, and leaving a greater fraction of residual char. The results are contrary to the reports on organically modified MMT clay based PP nanocomposites, as the catalytic degradation effect of acidic sites in clay accelerates the free radical degradation process of PP.[19]

The influence of the replacement of IFR by MA-ZrP and MP-ZrP at the same 25 phr global loading on thermal degradation of PP/JPP/IFR composites is compared in Figure 7. The thermal degradation of PP/JPP/IFR(25), PP/JPP/MA-ZrP(2)/IFR(23), and PP/JPP/MP-ZrP(2)/IFR(23) all occur in a three-stage process. The first two stages are ascribed to the development of an intumescent protective shield and the degradation of the polymeric matrix, while the third stage is due to the thermal degradation of the intumescent char. As seen from the DTG curve of PP/JPP/IFR(25) sample in Figure 7(B), the first maximum mass loss caused by the development of an intumescent structure occurs at 246°C (T_{1max}); the second maximum mass loss caused by the degradation of polymeric matrix occurs at 422°C (T_{2max}); on elevating the temperature, a broad peak centered at about 500°C (T_{3max}) appears due to the destruction of the intumescent char. PP/JPP/MA-ZrP(2)/IFR(23) and PP/JPP/MP-ZrP(2)/IFR(23) show a similar T_{1max}, but a remarkable 40°C increase in thermal stability compared with PP/JPP/IFR(25) in terms of T_{2max}; meanwhile, T_{3max} is also found to shift to higher temperature. Finally, MA-ZrP and MP-ZrP containing samples leave more residual chars.

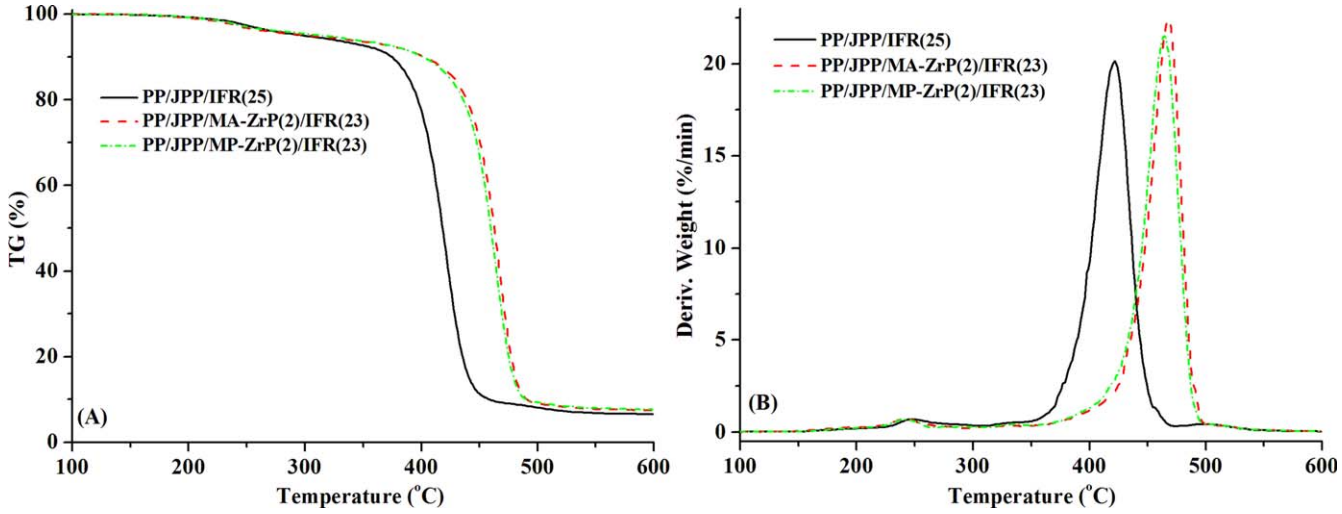

Figure 7. TGA and DTG curves of PP/JPP/IFR(25), PP/JPP/MA-ZrP(2)/IFR(23), and PP/JPP/MP-ZrP(2)/IFR(23) composites. [Color figure can be viewed in the online issue, which is available at wileyonlinelibrary.com.]

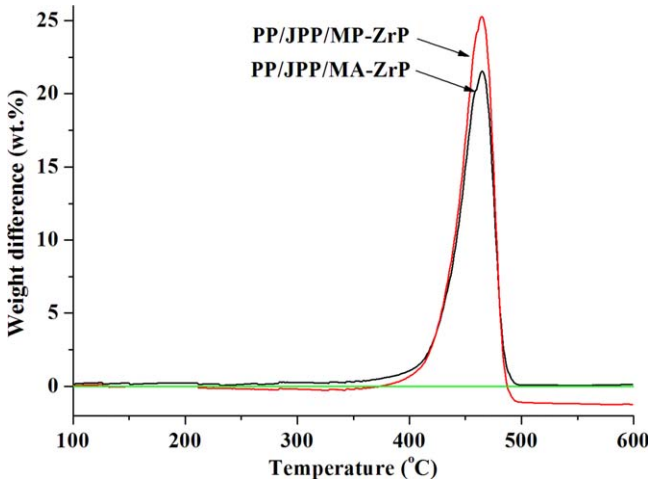

Figure 8. The weight difference curves between experimental and theoretical TGA curves of PP/JPP/MA-ZrP and PP/JPP/MP-ZrP composites. [Color figure can be viewed in the online issue, which is available at wileyonlinelibrary.com.]

Therefore, it can be concluded that adding MA-ZrP and MP-ZrP to PP or PP/IFR composites is favorable to enhance the thermal stability. It has been reported previously that the thermal and flammability performance of polymeric materials such as PS and poly(vinyl alcohol) are influenced by α-ZrP nanoplatelets through catalytic carbonization effect more than the physical effect.[6,20] However, as demonstrated in Figure 8, the weight differences between experimental and theoretical TGA curves of PP/JPP/MA-ZrP and PP/JPP/MP-ZrP composites (the curves of weight difference is calculated as TGA experimental curves minus the theoretical TGA curves, which are obtained by liner combinations of the experimental TGA curves of the single components, PP/JPP and MA-ZrP or MP-ZrP) demonstrate that although the hybrids show higher thermal stability in the relative high experimental temperature range, the introduction of MA-ZrP and MP-ZrP does not cause the polymeric matrix to yield more char; even worse, PP/JPP/MP-ZrP composite yields less char than expected. Therefore, the improvement in thermal stability is postulated to be mainly due to the physical effect of α-ZrP not a chemical effect through accelerating the charring process.

Flammability Studies

The cone calorimeter is one of the most effective bench-scale methods to study the flammability properties of materials; the parameters that are available include the HRR and especially its peak value, the time to ignition (t_{ign}), the time to peak HRR (t_p), the average specific extinction area (ASEA), the average mass loss rate (AMLR), and average effective heat of combustion (AEHC); finally, one can derive two parameters form cone data, the fire performance index (FPI, defined as t_{ign} divided by peak HRR [t_p]) and the fire growth rate (FIGRA, defined as peak HRR divided by t_p).

The dynamic HRR curves of MA-ZrP and MP-ZrP based PP composites are shown in Figure 9(A); the combustion data from the cone calorimeter are listed in Table III. PP/JPP blend burned rapidly after ignition and a HRR peak at 2655 kW m^{-2} appeared at 145 s. For PP/JPP/MA-ZrP and PP/JPP/MP-ZrP composites, they ignited earlier but the rate of heat release increased more slowly, and there was a 31% and 23% reduction in peak HRR, respectively, when compared with the PP/JPP blend. Correspondingly, the two samples showed lower AMLR, suggesting the decline of peak HRR was mainly due to the condensed phase flame retardant mechanism.

HRR curves of IFR flame retardant PP composites are shown in Figure 9(B). The rate of heat release of PP/JPP/IFR(25) increased sharply to a maximum of 560 kW m^{-2} at 65 s due to the development of intumescent shield, which was reduced by 79% compared with PP/JPP blend; followed by a plateau due to the intumescent protection from 65 to 180 s; then fell regularly.

Table III reveals that the hybrids in which the IFR is substituted by 2 phr of MA-ZrP and MP-ZrP exhibit an additional reduction in peak HRR. The HRR curves of PP/JPP/IFR composites containing MA-ZrP and MP-ZrP show similar features. Moreover, it

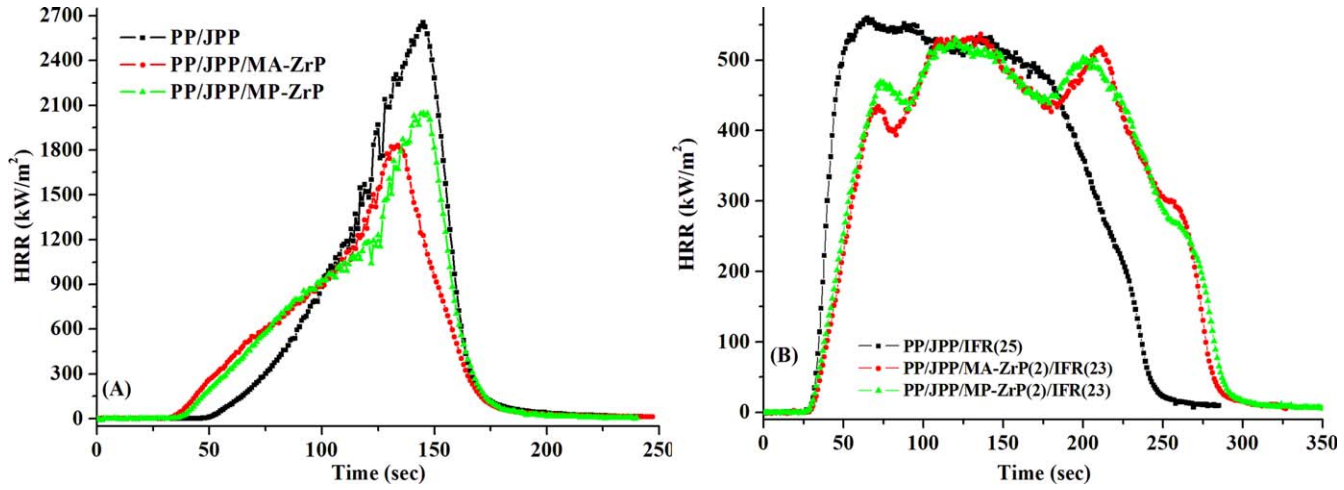

Figure 9. HRR curves of PP and its IFR flame retarded composites. [Color figure can be viewed in the online issue, which is available at wileyonlinelibrary.com.]

Table III. Cone Data of PP and Its IFR Flame Retarded Composites

Sample	Peak HRR (kW m^{-2})	t_p (s)	AEHC (MJ kg^{-1})	AMLR (g m^{-2} s^{-1})	t_{ign} (s)	ASEA (m^2 kg^{-1})	FPI ($\times 10^2$)	FIGRA
PP/JPP	2655	145	58	32	37	511	1.4	18.3
PP/JPP/MA-ZrP	1829	134	50	24	24	509	1.3	13.6
PP/JPP/MP-ZrP	2046	145	51	26	27	609	1.3	14.1
PP/JPP/IFR(25)	560	65	32	17	18	1244	3.2	8.6
PP/JPP/MA-ZrP(2)/IFR(23)	537	136	42	11	19	768	3.5	3.9
PP/JPP/MP-ZrP(2)/IFR(23)	530	120	43	11	17	769	3.2	4.4

HRR, heat release rate; t_p, time to peak HRR; AEHC, average effective heat of combustion; AMLR, average mass loss rate; t_{ign}, time to ignition; ASEA, average specific extinction area; FPI, fire performance index, t_{ign}/peak HRR; FIGRA, fire growth rate, peak HRR/t_p.

seems that the development of an intumescent shield occurs by a two-stage process; a sub-HRR peak appears at about 75 s then decreases and forms a stable intumescent shield at 105 s. Apparently, the intumescent shield exhibits more efficient fire protection than that from PP/JPP/IFR(25); they impart the hybrids longer total burning time and delay the time to HRR peak; as a result, these composites with modified α-ZrP exhibit lower fire growth rate (FPI). Table III also shows that ASEA values are 768 and 769 m^2 kg^{-1} for PP/JPP/MA-ZrP(2)/IFR(23) and PP/JPP/MP-ZrP(2)/IFR(23), respectively, which are decreased by 38% when compared with that of 1244 m^2 kg^{-1} for PP/JPP/IFR(25) composite, indicating the partially replacement of IFR by OZrP is of benefit to reduce the release of smoke.

Mechanism Postulation

Reassembly of layered-compound layers on sample surface by a forming lamellar physical barrier, which is driven by the gaseous products decomposed from the polymeric matrix, has an important role on thermal stability and flammability performance of polymeric materials.[21] In this study, the volatile thermal degradation products, such as NH_3 gases are produced inside the phosphate gallery spaces due to the decomposition of intercalated MA and MP at relatively low temperature,[22] and this is expected to push the phosphate layers apart and accumulate on the sample surface to efficiently form a barrier shield. As shown in Figure 6(B), a sub-DTG peak, appearing at about 470°C, can be found in both PP/JPP/MA-ZrP and PP/JPP/MP-ZrP composites; however, the barrier is not stable enough to sustain high temperature and bursts.

Meanwhile, the synchronization reactions between the cross-linking process of the IFR compositions and the isolation of gaseous products filling the intumescence play a key role on the development of intumescent char.[23] Due to the segregation of the phosphate barrier, volatilization is slow, which may lead to gaseous products, mainly NH_3, which can swell the char and help with the solidification of the char. Moreover, the stabilization effect of the phosphate layers may occur through the reaction between P—OH in α-ZrP and MPP. Both these together help to make an intumescent barrier with better thermal stability than that from PP/JPP/IFR. As a result, the composites with MA-ZrP and MP-ZrP exhibit higher thermal stability and flammability performance, meanwhile, transfer of the inside thermal degradation products into the flame zone is also prevented efficiently and results in a lower ASEA value.

CONCLUSIONS

The study was on the influence of OZrP, MA-ZrP, and MP-ZrP on PP and its intumescent flame retarded composites. PP/JPP/OZrP and PP/JPP/OZrP/IFR composites exhibited superior thermal stability and improved flammability performance compared with the PP/JPP blend and PP/JPP/IFR composite. It was postulated that the NH_3 produced inside the phosphate gallery space from the degradation of MA-ZrP and MP-ZrP is favorable to push the phosphate layers to accumulate on sample surface, functioning as a physical barrier. For PP/JPP/OZrP/IFR composites, the segregation effect of phosphate layers provided a positive effect on the development of intumescent structure by promoting the synchronicity between the cross-linking of the IFR compositions and the isolation of gaseous products filling the intumescence, which is favorable to improving the performance of intumescent char.

ACKNOWLEDGMENTS

This work was supported by the National Natural Science Foundation of China (No. 51276054) and the National Undergraduate Innovation and Entrepreneurship Training Programs (No. 201311059005 and 201311059006).

REFERENCES

1. Morgan, A. B.; Gilman, J. W. *Fire Mater.* **2013**, *37*, 259.
2. Zhao, C. X.; Sun, Z.; Liu, B. L.; Peng, G. *J. Macromol. Sci. B.* **2013**, *52*, 1453.
3. Enescu, D.; Alongi, J.; Frache, A. *J. Appl. Polym. Sci.* **2012**, *123*, 3545.
4. Cai, G. P.; Lu, H. D.; Xu, S. R.; Wang, Z. Z.; Wilkie, C.A. *Polym. Adv. Technol.* **2013**, *24*, 646.
5. Tai, Q. L.; Kan, Y. C.; Chen, L. J.; Xing, W. Y.; Hu, Y.; Song, L. *React. Func. Polym.* **2010**, *70*, 340.
6. Lu, H. D.; Wilkie, C. A.; Ding, M.; Song, L. *Polym. Degrad. Stabil.* **2011**, *96*, 1219.
7. Laoutid, F.; Bonnaud, L.; Alexandre, M.; Lopez-Cuesta, J. M.; Dubois, P. *Mater. Sci. Eng. R.* **2009**, *63*, 100.

8. Lenza, J.; Merkel, K.; Rydarowski, H. *Polym. Degrad. Stabil.* **2012**, *97*, 2581.
9. Yen, Y. Y.; Wang, H. T.; Guo, W. J. *J. Appl. Polym. Sci.* **2013**, *130*, 2042.
10. Kaynak, C.; Gunduz, H. O.; Isitman, N. A. *J. Nanosci. Nanotechnol.* **2010**, *10*, 7374.
11. Modesti, M.; Lorenzetti, A.; Besco, S.; Hreja, D.; Seenzato, S.; Bertani, R.; Michelin, R. A. *Polym. Degrad. Stabil.* **2008**, *93*, 2166.
12. Yang, D. D.; Hu, Y.; Song, L.; Nie, S. B.; He, S. Q.; Cai, Y. B. *Polym. Degrad. Stabil.* **2008**, *93*, 2014.
13. Tang, Y.; Hu, Y.; Wang, S. F.; Gui, Z.; Chen, Z. Y.; Fan, W. C. *Polym. Inter.* **2003**, *52*, 1396.
14. Guo, J. B.; He, M.; Li, Q. F.; Yu, J.; Qin, S. H. *J. Appl. Polym. Sci.* **2013**, *129*, 2063.
15. Sun, L. Y.; Boo, W. J.; Sue, H. J.; Clearfield, A. *New J. Chem.* **2007**, *31*, 39.
16. Hayashi, A.; Nakayama. H.; Tsuhako, M. *Solid State Sci.* **2009**, *11*, 1007.
17. Wang, H. N.; Liu, W. J.; Yao, W.; Zhang, K.; Zhong, J.; Chen, R. Y. *Appl. Surf. Sci.* **2013**, *268*, 179.
18. Lu, H. D.; Wilkie, C. A.; Ding, M.; Song, L. *Polym. Degrad. Stabil.* **2011**, *96*, 885.
19. Ramos, F. G. R.; Melo, T. J. A.; Rabello, M. S.; Silva, S. M. L. *Polym. Degrad. Stabil.* **2005**, *89*, 383.
20. Yang, D. D.; Hu, Y.; Xu, H. P.; Zhu, L. P. *J. Appl. Polym. Sci.* **2013**, *130*, 3038.
21. Kashiwagi, T.; Harris, R. H., Jr; Zhang, X.; Briber, R. M.; Cipriano, B. H.; Raghavan, S. R.; Awad, W. H.; Shields, J. R. *Polymer* **2004**, *45*, 881.
22. Laoutid, F.; Bonnaud, L.; Alexandre, M.; Lopez-Cuesta, J.-M.; Dubois, *Ph. Mater. Sci. Eng.* **2009**, *63*, 100.
23. Gibov, K. M.; Mamleev, V. S. *J. Appl. Polym. Sci.* **1997**, *66*, 329.